RESEARCH PAPER

In vivo toxicity and antimicrobial activity of AuPt bimetallic nanoparticles

Daniela Maria Ducatti Formaggio · Xisto Antonio de Oliveira Neto ·
Lina Dayse Alcântara Rodrigues · Vitor Martins de Andrade · Bruna C. Nunes ·
Mônica Lopes-Ferreira · Fabiana G. Ferreira · Cristiane C. Wachesk ·
Emerson R. Camargo · Katia Conceição · Dayane Batista Tada

Abstract Despite the potential antimicrobial activity of metallic nanoparticles, the increasing concerns about nanosafety have been holding back the use of these materials in therapeutics and biomedical devices. In the last years, several studies called attention to metallic nanoparticles toxicity. In the most part of in vitro studies performed with mammalian cells, metallic NPs reduced cell viability and induced genotoxicity and inflammatory responses. Bimetallic NPs have attracted great attention because they present distinct and even more advanced characteristics when compared to nanoparticles formed by a single metal. Recently, bimetallic NPs have emerged as an alternative to improve the antimicrobial activity of metallic nanoparticles, aiming at the broadening of the action spectrum and the reduction of the toxicity. However, the biocompatibility of bimetallic nanoparticles has been demonstrated only by in vitro studies. In the present work, the toxicity of AuPt nanoparticles was addressed both in vitro and in vivo. In addition, the antimicrobial activity of AuPt bimetallic nanoparticles has been evaluated in comparison with Au and Ag nanoparticles. The nanoparticles were characterized by ultraviolet-visible spectroscopy, dynamic light scattering, transmission electron microscopy, inductively coupled plasma optical emission spectroscopy, and X-ray diffraction. The antimicrobial activity was studied against *Candida albicans*, *Pseudomonas aeruginosa*, and *Staphylococcus aureus*. The toxicity of nanoparticles was evaluated in vitro by analyzing their toxicity against human fibroblast cells (HS68 cell line) and in vivo by embryonic toxicity test in zebrafish (*Danio rerio*). The results confirmed the intrinsic antimicrobial activity of the three types of nanoparticles but different toxicity. Bimetallic nanoparticles showed enhanced antimicrobial activity in comparison with Au nanoparticles but lower antimicrobial activity compared with Ag nanoparticles. However, AuPt nanoparticles showed great advantage over Ag nanoparticles due to the absence of cytotoxicity and lower toxicity in vivo.

D. M. D. Formaggio · L. D. A. Rodrigues · B. C. Nunes ·
F. G. Ferreira · C. C. Wachesk · D. B. Tada (✉)
Laboratory of Nanomaterials and Nanotoxicology, Universidade Federal de São Paulo, Rua Talim, 300 São José dos Campos, São Paulo, Brasil
e-mail: d.tada@unifesp.br

X. A. de Oliveira Neto · V. M. de Andrade · K. Conceição
Laboratório de Bioquímica de Peptídeos, Universidade Federal de São Paulo, Rua Talim, 300 São José dos Campos, São Paulo, Brazil

M. Lopes-Ferreira
Immunoregulation Unit of the Special Laboratory of Applied Toxinology (CeTICS, CEPID/FAPESP), Instituto Butantan, Avenida Vital Brasil, 1500, São Paulo, Brazil

E. R. Camargo
Department of Chemistry, UFSCar–Federal University of São Carlos, Rod. Washington Luis, km 235, São Carlos 13565-905, Brazil

🌐 Springer

Introduction

Metallic nanoparticles (NPs) have been extensively explored in health sciences as diagnostic and therapeutic agents (Smith et al. 2012; Yao et al. 2016; Song et al. 2013; Linic et al. 2015; Aioub et al. 2017). Even more remarkable has been the investigation of the antimicrobial activity of metallic NPs which has been motivated by the emergence and re-emergence of infectious diseases due to multidrug resistance of pathogenic microorganisms. In addition to the enhanced antimicrobial activity, the high stability of metallic NPs is another advantage over the organic compounds normally used as antimicrobial drugs (Singh et al. 2018; Siddiqi et al. 2018; Wang et al. 2017). The antimicrobial efficiency of metallic NPs depends mainly on the chemical nature, surface chemistry, and charge of the NPs. Although the mechanism of action of NPs has not been entirely elucidated, the antimicrobial activity has been associated with the interaction between NPs and the microbial membrane together with oxidative stress (Siddiqi et al. 2018; Dakal et al. 2016; Feng et al. 2015). Among the most efficient antimicrobial NPs, Au and Ag NPs have attracted a special attention as antibacterial agents. It is believed that antibacterial activity of Au and Ag NPs is not only a consequence of the interaction between NPs and bacterial membrane but also due to enzymes inactivation by the binding of thiol groups to gold and silver atoms (Hinterwith et al. 2012; Park et al. 2018; McShan et al. 2014; Kumar et al. 2013).

Bimetallic NPs are composed of two different metal elements forming a single nanometric material. These NPs have attracted great attention because they present distinct and improved features when compared with NPs formed by a single metal including enhanced antimicrobial and catalytic activity. The uniqueness of bimetallic NPs is related mainly to the synergism between the constituent metals and to their large surface area (Xu et al. 2015; Srinoi et al. 2018). Among the most commonly studied bimetallic, NPs are the ones composed by noble metals (Au, Ag, Pt, and Pd) or transition metals (Ni, Cu, Fe, Co). The properties of bimetallic NPs depend closely on their atomic arrangement and electronic structure (Xu et al. 2015; Lai et al. 2010). Several atomic arrangements can be obtained according to the composition, the reaction conditions, and the synthetic route (Lapp et al. 2018). Notably, the synthesis of bimetallic NPs presents a greater challenge due to inherent peculiarities of each metal introduced into the system, such as its different redox potentials and chemical reactivity. Thus, recently many researchers have reported improvements in the synthesis of bimetallic NPs in solution (Srinoi et al. 2018; Qingbo et al. 2010).

Despite the potential antimicrobial activity hold by metallic NPs, the increasing concerns about nanosafety have hampered the translation of these NPs to the therapeutic and biomedical fields. In the last years, several studies called attention to the metallic NPs toxicity. The toxic effects were cell line dependent but in the most part of in vitro studies performed with mammalian cells it was observed that metallic NPs reduced cell viability and induced genotoxicity and inflammatory responses (Gao et al. 2017; Kaiser et al. 2017; Kim et al. 2011; Asharani et al. 2011; Ávalos Fúnez et al. 2013; Arvizo et al. 2010). The extent of toxic effect was dependent on the metallic nature and on the surface functional groups. Severe effects were observed with Ag NPs which induced membrane leakage and decrease in mitochondrial activity in pulmonary, dermal, and hepatoma fibroblasts (Ávalos Fúnez et al. 2013).

The interaction of different types of NPs with humans, animals, plants, and aquatic organisms are commonly addressed through in vitro assays with the use of reconstituted cell membranes and animal cells. Although in vitro assays indicate a promising direction, in vivo assays are closer to the clinical application, can be explored systemically, and directly reflect the adaptation and damage of the organism. Regarding in vivo assays, in addition to the commonly used mice, rats or rabbits, zebrafish (Danio rerio) has been widely used in nanotoxicological studies. The use of this experimental model has grown in recent years due to its low cost, small size (3 to 4 centimeters), high fertilization rate, fast life cycle, and embryo transparency (Asharani et al. 2011; Howe et al. 2013; Ma et al. 2018; Van Pomeren et al. 2017; Sieber et al. 2017). By using zebrafish as animal models, Asharani et al. (2017) showed that AgNPs were the most toxic NPs in comparison with PtNPs and AuNPs. Both AgNPs and PtNPs showed a drop in heart rate, touch response, and axis curvature. In addition, AgNPs also induced pericardial effusion, abnormal cardiac morphology, circulatory defects, and absence or malformation of the eyes. None of these toxic effects was observed for AuNPs.

In contrast to many reports addressing metallic NPs, the number of works on the biological interaction of bimetallic NPs is still limited. Nevertheless, the comparison between the toxicity data is hampered by the

differences in the physicochemical characterization and in the units used to represent NPs concentration. In some works, concentration was reported as a number of particles/volume, calculated by using the plasmon band. In others, the concentration was reported as molar concentration of metal, which was calculated based on the amount of metal ions added in the reaction medium considering 100% of reduction. Additionally, in most part of comparative works, NPs concentration is normalized by concentrating or diluting NPs stock suspension obtained from the synthetic process. However, we should consider that any change in the concentration of stock NPs suspension changes the colloidal state and consequently alters the toxic effect and antimicrobial activity. The present work aims at the investigation of the biological interaction of bimetallic NPs of gold and platinum (AuPtNPs) in aqueous suspension. All the studies were performed in comparison with AuNPs and AgNPs. The NPs suspension used in all the assays were the one obtained directly from the synthesis in order to maintain the colloidal state of the NPs.

The antimicrobial activity of the NPs was studied against *Candida albicans*, *Pseudomonas aeruginosa*, and *Staphylococcus aureus*. The NPs biological activity was evaluated in vitro by analyzing their toxicity against human fibroblast cells (Hs68 cell line) and in vivo by embryonic toxicity test in zebrafish (*Danio rerio*).

Materials and methods

Synthesis of nanoparticles

Synthesis of AuNPs

Tetrachloroauric (III) acid (HAuCl$_4$.3H$_2$0 ≥ 99.9% trace metal basis) and trisodium citrate dihydrate (≥ 99.9%) were ordered from Sigma-Aldrich. Chemicals were used as provided and ultrapure water was used for all procedures.

AuNPs were prepared according to the traditional Turkevich method (Enustun and Turkevich 1963), which is based on the reduction of gold ions by the trisodium citrate in aqueous solution. In an Erlenmeyer, 1 L of ultrapure water was heated to 95 °C on a hot plate with constant stirring. Subsequently, 20 mL of a precursor solution (HAuCl$_4$.3H$_2$O) in the water at 5.0×10^{-2} M was quickly added followed by the addition of 10 mL of a sodium citrate aqueous solution at 3.0×10^{-1} M. The

stoichiometric ratio between the metal salt and the reducing agent was of 1:3 and the pH was 3.0. After the color of the solution had changed, it was heated for ~ 12 min until it turned to the characteristic wine-red, indicating the formation of AuNPs. The hot plate was switched off and the solution was cooled at room temperature. The NPs suspension was then transferred into a glass bottle for storage at 4 °C.

Synthesis of AgNPs

Silver nitrate (≥ 99.9% trace metal basis) and trisodium citrate dihydrate (≥ 99.9%) were ordered from Sigma-Aldrich. Chemicals were used as provided and ultrapure water was used for all procedures.

AgNPs were prepared according to the traditional Turkevich method (Enustun and Turkevich 1963), the same used to synthesize AuNPs, with some adjustments suggested by Gorup et al. (Gorup et al. 2011). In an Erlenmeyer, a volume of 100 mL of 1.0 mM aqueous silver nitrate solution was heated to 90 °C on a hot plate with constant stirring. Subsequently, 1.0 mL of 0.3 M aqueous sodium citrate solution was quickly added. The stoichiometric ratio between the metal salt and the reducing agent was 1:3 and the pH was about 8.2. After the color of the solution had changed, it was heated for 13 min until it turned yellowish, indicating the formation of AgNPs. Lastly, 1.0 mL of 1.4 M aqueous ammonia solution was added to stabilize and generate AgNPs suspension with narrow-size distribution. The hot plate was switched off and the solution was cooled at room temperature. The NPs suspension was then transferred into a glass bottle for storage at 4 °C.

Synthesis of AuPtNPs

Tetrachloroauric (III) acid (HAuCl$_4$.3H$_2$0; ≥ 99.9% trace metal basis), potassium tetrachloroplatinate (II) (K$_2$PtCl$_4$; 98% trace metal basis) and polyethylene glycol sorbitan monooleate (Tween 80) were ordered from Sigma-Aldrich.

AuPtNPs were synthesized by following the procedure described by Zhao et al. (Zhao et al. 2014). A mixture of HAuCl$_4$·3H$_2$O at 0.01 mmol, K$_2$PtCl$_4$ at 0.0025 mmol and 40 mg Tween 80 was stirred in 10 mL of water for 30 min in an ice-water bath. After all reagents have been dissolved, the solution was heated to 100 °C on a hot plate with constant stirring. After approximately 15 min, the reducing agent (NaBH$_4$;

1.54 mg) was slowly added to the mixture under vigorous stirring. After the solution's color had changed, the temperature was switched off but the NPs suspension was kept under gentle stirring for one hour within an ice-water bath. Finally, the suspension was dialyzed (25 kDa molecular weight cut off) for 24 h against deionized water. The suspension was then transferred into a glass bottle and stored at 4 °C.

Dynamic Light Scattering

Dynamic light scattering (DLS) measurements were performed in a Beckman Coulter Delsa Nano equipment. In the size analysis, NPs suspensions were diluted in water and in the analysis of zeta potential, NPs suspension were used without dilution. Values of hydrodynamic diameter were calculated by using Stokes-Einstein equation and the particle size distributions were obtained by the autocorrelation function CONTIN, available in the Delsa Nano UI software 3.73.

UV-Vis

UV-Vis spectra of NPs were obtained in a spectrophotometer V-730 (JASCO Inc.) by using water as a reference sample. The measurements were done in the range of 200–800 nm with a step of 1 nm and a rate of 400 nm/min. All the samples were analyzed without dilution.

Inductively coupled plasma-optical emission spectroscopy

The composition of NPs was determined by inductively coupled plasma-optical emission spectroscopy (ICP-OES) in a spectrometer Arcos with radial-view (Spectro, Inc.). The samples were previously centrifuged and ressuspended in water, without dilution or drying. The analysis was performed by the Central Analítica in the Institute of Chemistry-University of São Paulo (Brazil).

Transmission eletronic microscopy

The size and morphology of NPs were determined by transmission electronic microscopy (TEM). The NPs suspension was dropped on Cu grids coated with carbon film and dried at room temperature. A microscope TECNAI (FEI) at 120 kV was used to characterize the NPs at IEAMAR-University of the State of São Paulo (UNESP). High-resolution TEM was performed in a

FEI microscope TECNAI G2 TF20 XT available at Federal University of São Carlos (UFSCAR/ FAPESP 2013/07296-2).

X-ray diffraction

X-ray diffraction analysis was performed at the Laboratório Associado de Sensores e Materiais (LABAS) from Instituto Nacional de Pesquisas Espaciais (INPE-SJC), in a diffratometer Philips, X-Pert PRO PANalytical ((λ = 1.5406 Å) at 45 kV, 40 mA, step of 0.02°, range of 40°–130° at 2θ). The samples were previously lyophilized in an equipment SpeedVac (miVac, GeneVac).

Antimicrobial activity test

The antimicrobial activity was monitored by a liquid growth inhibition assay against *Staphylococcus aureus* (ATCC 6538), *Pseudomonas aeruginosa* (ATCC 15442) and *Candida albicans* (ATCC 10231), as described by Conceição et al. (Conceição et al. 2012) with modifications. Pre inocula of the strains were prepared in Brain Heart Infusion-BHI (KASVI) and incubated at 37 °C in a shaker. Different concentrations (Table 1) of NPs were added in a 96-wells microplate with 100 μL of microorganism suspension (the final density of bacteria was of 10^6 CFU/mL) in each well. In each well, the total volume was completed to 200 μL with BHI medium and the plate was incubated at 37 °C. Streptomycin sulfate salt (Sigma-Aldrich) and ultrapure water were used as positive and negative control, respectively. It is noteworthy

Table 1. Concentration of NPs incubated with microorganisms

Vol. of NPs in the well (μL)	[Metal] (mM)			[metal] (μg/mL)		
	AuNPs	AgNPs	AuPtNPs	AuNPs	AgNPs	AuPtNPs
100.0	0.96	0.20	0.69	189.0	21.4	136.0
50.0	0.48	0.10	0.34	94.4	10.7	68.0
25.0	0.24	0.05	0.17	47.2	5.3	34.0
12.50	0.12	0.02	0.09	23.60	2.67	17.0
6.25	0.06	0.01	0.04	11.80	1.34	8.50
3.12	0.03	0.006	0.02	5.90	0.67	4.20

that for each set of assay where a certain volume of NPs suspension was added to each well (Table 1), the same volume of water was added in the negative control in order to eliminate any inhibition effect from the dilution of the culture medium. After incubation for 24 h, the bacterial growth was quantified by measuring the absorbance at 630 nm (plate reader Synergy, Biotek Instruments). The inhibition of bacterial growth was calculated by considering the negative control as 100% of growth, or, 0% of inhibition.

Intracellular ROS generation

The ROS generation was monitored by 2',7'-dichlorofluorescin diacetate (DCFDA) oxidation method by using *S. aureus* (ATCC 6538), *P. aeruginosa* (ATCC 15442), and *C. albicans* (ATCC 10231. Pre inocula of the strains were prepared in Brain Heart Infusion - BHI (KASVI) and incubated at 37 °C in a shaker. Following, 100 μL of each type of NPs suspension (Table 1) were added in a 96-well microplate with 100 μL of microorganism suspension (the final density of bacteria was of 10^6 CFU/mL) in each well and incubated at 37 °C. Streptomycin sulfate salt (Sigma-Aldrich) and ultrapure water were used as a positive and negative control, respectively. After incubation for 24 h, the microorganisms were incubated with 5 μM of DCFDA for 1 h. Then, a solution of 1% of SDS was added in order to lyse the cells and DCF fluorescence was measured in a plate reader (λexc = 485 nm; λem = 528 nm).

Cell viability assays

The Hs68 cell line was cultured in DMEM medium supplemented with 10% FBS. A density of 5×10^3 cells per well was placed in 96-wells microplates and incubated for 12 h. Then, the medium was replaced with the medium containing different concentrations of AuNPs, AgNPs, and AuPtNPs. The cells were incubated with NPs at different concentrations (Table 2) for 24 h, 48 h, and 72 h. The NPs were used at the concentration of stock suspension and dilutions of 2×, 5×, 10×, and 100× in order to assess the toxicity of each type of NP at the colloidal state resultant from the commonly used synthetic routes. Cells incubated with the culture medium without NPs were used as a negative control. After treatment, the samples were replaced by 100 μL of MTT aqueous solution (2 mg/mL) and incubated for 4

Table 2. Concentration of the samples used in the in vitro and in vivo assays

NP	Sample	Dilution	[Metal]/mM
AuNP	Stock suspension	–	1.91
	Dilution 1	10×	0.19
	Dilution 2	100×	0.01
AgNP	Stock suspension	–	0.39
	Dilution 1	2×	0.19
	Dilution 2	5×	0.07
AuPtNP	Stock suspension	–	1.38
	Dilution 1	2×	0.69
	Dilution 2	5×	0.27

h. The MTT solution was removed, and 100 μL of DMSO was added to solubilize the formazan. The formazan was quantified by measuring the absorbance at 540 nm. The cell viability was calculated by considering the negative control as 100% of cell viability. All experiments were performed in septuplicate. All results are presented as mean values and standard deviation. Statistical analyses were done by one-way analysis of variance.

Zebrafish embryos assay

This study was performed in strict accordance with the recommendations provided by the Brazilian Association of Technical Standards (ABNT) NBR 15088/2016 (ABNT_2016). The protocols used in this assay were described in Busquet et al. (Busquet et al. 2014). NPs suspensions at different concentrations (Table 2) were freshly prepared by diluting stock suspension in E2 medium for zebrafish. For each concentration of NPs, three replicates were prepared. The assay was carried out in 24-well polystyrene microplates, placing five embryos per well in 2 mL of E2 medium containing the NPs. Five embryos in ultrapure water were used as positive control and five embryos in E2 medium were used as a negative control. Exposures to NPs were conducted at 28 °C in an incubator. The development of the zebrafish embryos was evaluated after 24 h, 48 h, 72 h, and 96 h of incubation by using a stereo microscope Luma V12–Zeiss. Three main aspects of toxicity were evaluated and scored, namely, mortality, morphological developmental defects, and teratogenic effects.

Results and discussion

Characterization of the NPs

The morphology and size distribution of NPs were evaluated by TEM. The images (Fig. 1) showed that AuNPs and AuPtNPs were predominantly spherical and homogenous in size. AgNPs were predominantly spherical, the presence of NPs with cylindrical and triangular shapes was notable. The mean diameter calculated from the TEM images are shown in Table 3.

Due to the small size of AuPtNPs, these NPs were further characterized by HRTEM. The image presented in Fig. 1d showed the crystalline atomic structure of AuPtNPs. These NPs were spherical but aggregated into cylindrical structures. The red circles in the TEM images highlight the union of two spheres. The crystalline structure of the aggregates suggests that the aggregation of AuPtNPs is a process of coarsening via orient attachment. Oriented attachment of NPs has been primarily observed in the merge process of TiO_2 NPs (Penn and Banfield 1998) and the mechanism of coarsening was unveiled both by HRTEM and Molecular dynamics (Raju et al. 2014). Following, orient attachment was

extended to explain the aggregation of NPs with different compositions and today it is known to take place when two neighbors NPs have identical crystallographic configurations (Murphy et al. 2015; Qian et al. 2015).

The NPs were further characterized by dynamic light scattering (DLS). The hydrodynamic diameter, polydispersity, and zeta-potential are depicted in Table 3. As expected, the hydrodynamic diameter is higher than the diameter calculated from TEM images since this analysis is performed with dried samples and the DLS measurements require NPs in suspension. Besides, hydrodynamic diameter is a measurement of NPs diameter together with the electric dipole layer adhered to their surface. The measurement of hydrodynamic diameter of AuPtNPs by DLS was not possible since these NPs were too small to be detected by the equipment. Nevertheless, the DLS was useful to measure AuPtNPs zeta potential. All the NPs presented negative zeta potential with high values in module, which suggested NPs suspension of high stability. The satisfactory stability was also evidenced by the low value of polydispersity index of AuNPs and AgNPs.

The homogeneity of size distribution of AuNPs and AgNPs was also evidenced by the narrow plasmon band

Fig. 1 TEM images of AuNPs, AuPtNPs, AgNPs

(a) AuNPs

(b) AgNPs

(c) AuPtNPs

(d) AuPtNPs
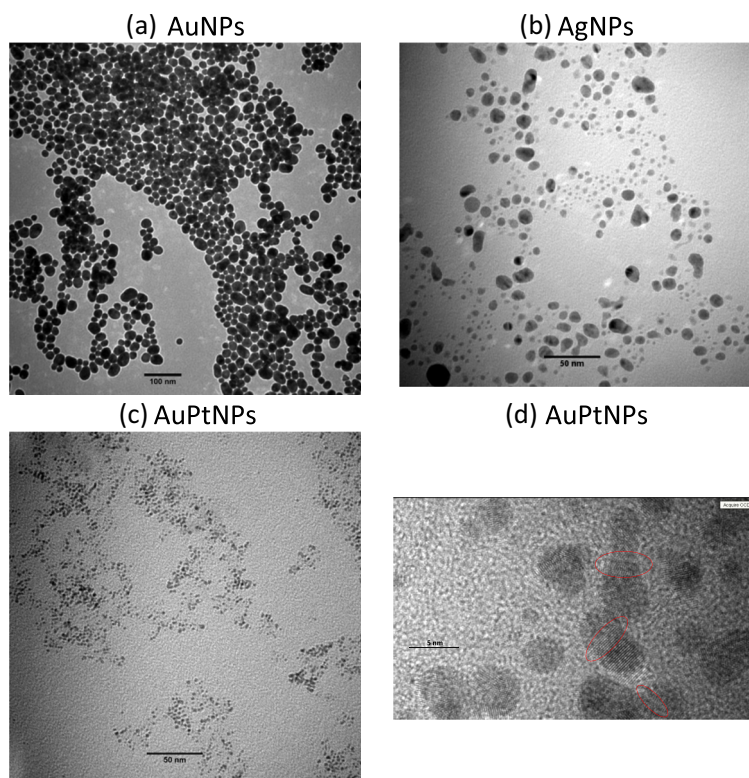
Table 3. Values of diameter, hydrodynamic diameter, polydispersity index (PDI), and zeta-potential of metallic NPs

NP	TEM diameter/nm	Hydrodynamic diameter/nm	PDI	Zeta potential/mV
Au	19 ± 8	23 ± 8	0.21	− 45 ± 4
Ag	4 ± 2	30 ± 8	0.24	− 36 ± 1
AuPt	2 ± 1	–	–	− 21 ± 2

identified by UV-Vis characterization (Fig. 2). The plasmon band of AuNPs was observed at 520 nm and that of AgNPs was observed at 420 nm. According to Haiss et al. (Haiss et al. 2007) and Paramelle et al. (Paramelle et al. 2014), these values and the value of absorbance at the plasmon band can be correlated to the concentration and size of these NPs. The concentration of AuNPs was calculated as being 0.46×10^{-8} M. According to Paramelle et al., the maximum absorbance at 420.9 nm corresponds to AgNPs of 50 nm, which disagrees with the diameter measured herein by TEM ($d = 4$ nm). Even so, the value of the molar extinction coefficient calculated by Paramelle et al. was used in order to calculate the molar concentration. By using the value of 537 M^{-1} cm^{-1} 10(Enustun & Turkevich, 1963), the concentration of AgNPs was calculated as being of $4.3.10^{-11}$ M. The plasmon band was absent in the UV-Vis spectra of AuPt NPs, which is in line with the results obtained by Zhao et al. (Zhao et al. 2014). Although the absence of the characteristic plasmon band of Au in the UV-Vis spectrum of AuPt NPs has been considered an indicative of the core-shell structure where the core is composed by gold and the shell by platinum (Westsson and Koper 2014), it is noteworthy that the UV-Vis is a limited technique for the characterization of NPs structure since it identifies only the metals present at the NPs surface besides being variable with NPs size and shape.

Since there is no correlation between UV-Vis spectra of AuPtNPs and NPs concentration, in order to report NPs suspension at the same unit, the concentration of the three
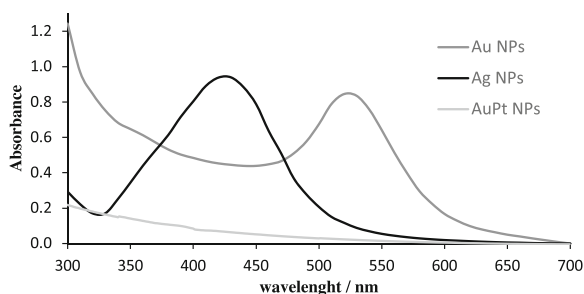
Fig. 2 UV-Vis spectra of AuNPs, AuPtNPs, AgNPs

types of NPs suspension was quantified by ICP-OES. Thus, the concentration was reported as molar concentration of metals. Table 4 depicts the values of concentration of each type of NP suspension in molar of total metal. Besides, for comparative purposes, the concentrations in molar of NPs of AuNPs and AgNPs were also shown in Table 4.

The AuPtNPs were further characterized by X-ray diffraction (XRD) in order to gain insights on the NPs atomic structure. The XRD pattern of AuPtNPs was compared with the XRD pattern of Au (Fig. 3) and with the XRD pattern of Pt ($2\theta = 39.7°$, $46.2°$, $67.4°$, and $81.2°$) from the Powder Diffraction File databank. The main diffraction peaks of AuNPs ($2\theta = 38.3°$, $44.6°$, $64.7°$, and $77.5°$) could be assigned to the fcc atomic structure. None of the peaks identified in the AuPtNPs diffractogram ($2\theta = 38.4°$, $45.4°$, $56.5°$, $65.7°$, and $78.9°$) was coincident with the peaks of pure metals. Even if the resolution of the XRD is not enough to provide accurate information regarding the distribution of the elements into the NP, it is a very useful technique to discriminate the presence of alloys or pure metals into the NP. The presence of pure metals, both in a simple mixture of pure metallic NPs or in a core-shell structure, would result in a diffractogram containing at least the peaks of one of the metals. Since the peaks of AuPtNPs had intermediary values between pure AuNPs and PtNPs, the XRD supports our claim that the synthesis of AuPtNPs resulted in an alloy structure of Au and Pt atoms. Indeed, Au and Pt alloying at nanoscale has been proved by recent works through experimental and computer simulations (Uson et al. 2015; Zhao et al. 2013; Zhong et al. 2008; Petkov et al. 2012; Mott et al. 2007). Their results showed the fcc crystalline atomic structure of

Table 4. Concentration of metals in the NPs suspension

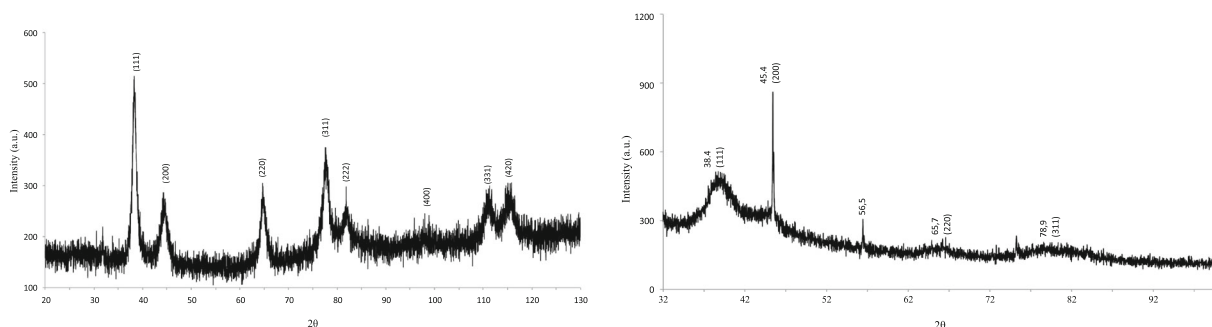| NP	[Metal]/mM	[NPs]/M
Ag	0.39	4.3×10^{-11}
Au	1.91	4.6×10^{-9}
AuPt	1.38 ([Au] = 1.10 mM) ([Pt] = 0.28 mM)	–

Fig. 3 DRX diffraction of AuNPs and AuPtNPs

AuPtNPs at the range of 2–10 nm. According to Zhao et al. (Zhao et al. 2013), a 0.11° shift of the (111) peak to higher 2θ angle from pure Au and a 1.58° shift to lower 2θ angle from pure Pt are characteristics of a AuPt single-phase alloy. In addition, AuPt nanoalloys have been characterized to have smaller inter-atomic distances compared to the bulk materials (Zhong et al. 2008). Furthermore, the mean square displacements of atoms are reduced from the inner part of the NP to the surface (Petkov et al. 2012). Most likely, these features endow bimetallic NPs enhanced catalytic and antimicrobial activities.

Owing the complexity of atomic structure of AuPtNPs, the phase type of these NPs cannot be directly identified by DR-X analysis. Thus, a combination of several techniques has been applied by researchers aiming at the phase identification of AuPt nanoalloy. By coupling atomic pair distribution functions (PDFs) to high-energy X-ray diffraction, Petkov et al. (Petkov et al. 2012) calculated a lattice parameter of 4.023 to AuPt NPs composed by 20% Pt and 80% of Au. Since this composition was obtained by ICP-OES as also performed to the AuPtNPs synthesized herein, the lattice parameter of our AuPtNPs was also considered as 4.023. According to Mott et al. (Mott et al. 2007), this lattice parameter corresponds to 37% of Pt in AuPt alloy. Nevertheless, the authors suggested that EDX analysis would be the most accurate technique to identify the AuPt alloy phase. So, herein, EDX analysis done by using HRTEM images indicated 19% of Pt and 81% of Au, which is very similar to the composition measured by ICP-OES. Therefore, it was concluded that AuPtNPs synthesized herein had a single $Au_{81}Pt_{19}$ phase alloy structure.

Minimal inhibitory concentration

Antimicrobial activity of AuNPs, AgNPs, and AuPtNPs was evaluated against three types of bacteria (*S. aureus*, *P. aeruginosa*, *E. coli*) and one type of fungus

(*C. albicans*). The inhibitory effect of these NPs on the growth of the microorganisms was monitored by measurement of optical density (OD) at 630 nm. The monitoring of microbial growth is commonly performed by OD measurement at 595–600 nm; however, at this range, the value of OD is influenced by the plasmon band of AuNPs. By choosing 630 nm, we ensured that the value of OD was proportional to the microbial concentration.

The values of concentration of each type of NP required to inhibit 40% of microbial growth are depicted in Table 5. As expected, the AgNPs were the most efficient since at a concentration lower than 0.02 mM, these NPs inhibited the growth of all the tested microorganisms. This concentration was about 3 to 6 times lower than the concentration of AuNPs or 2 to 4.5 times lower than the concentration of AuPtNPs required to inhibit the microbial growth. For example, in order to inhibit the growth of *P. aeruginosa* it was required 0.02 mM of AgNPs whereas AuPtNPs only showed the inhibition at 0.09 mM. The efficiency was even lower for AuNPs which inhibited *P. aeruginosa* growth at 0.12 mM. Notably, for S. aureus inhibition, AuPtNPs showed the same activity than AgNPs since both NPs inhibited the bacterial growth at the concentration of 0.02 mM. The remarkable antimicrobial activity of AgNPs is associated with multiple mechanisms of ac-

Table 5. Values of concentration of NPs required to inhibit at least 40% of microbial growth

Microorganism	[Metal]/ mM		
	AuNPs	AgNPs	AuPtNPs
S. aureus	0.06	0.02	0.02
P. aeruginosa	0.12	0.02	0.09
E. coli	0.06	0.01	0.04
C. albicans	0.06	0.01	0.04

tion including damaging of cellular membrane, release of ions Ag$^+$, unbalance of cell metabolism, ROS generation, and direct interaction with proteins via thiol groups (Siddiqi et al. 2018; Zhou et al. 2012; Jung et al. 2008; Tian et al. 2018; Villiers et al. 2010). The antimicrobial efficiency of AuPt NPs was higher than the activity of AuNPs, which is in line with Zhao et al. who showed antimicrobial activity of AuPtNPs and AuNPs against *E. coli*, multidrug-resistant *E. coli*, *P. aeruginosa*, *K. pneumoniae*, and *S. choleraesius*. As observed herein, they also reported enhanced antimicrobial activity of AuPt NPs in comparison with AuNPs.

Although the antimicrobial activity of metallic NPs has been already reported in several works, the comparison of our value of MIC with the values reported before is hampered by the different units used to represent NPs concentration. In some works, concentration was reported as number of particles/volume, in others as concentration of metal/volume, which was commonly calculated based on the amount of metal ions added in the reaction medium and not by quantitative measurement by ICP-OES.

In vitro ROS generation by NPs

The remarkable antimicrobial activity displayed by AgNPs has been associated to multiple mechanism of action, including NPs insertion into the cell membrane, causing membrane disruption, release of Ag$^+$ ions from AgNPs, unbalance of cell metabolism due to AgNPs interaction with biomolecules and oxidative stress caused by AgNPs ROS generation (Singh et al. 2018; Siddiqi et al. 2018; Wang et al. 2017; Dakal et al. 2016).

On the other hand, there is no information regarding the mechanism of action of AuPtNPs, and only one work was found to report the antimicrobial activity against a limited number of bacteria(Raju et al. 2014). In order to gain some insight regarding the mechanism of action of AuNPs, AgNPs, and AuPtNPs, the ROS generation was measured in vitro with different types of microorganisms. Figure 4 shows the values of fluorescence intensity measured in each type of microorganism after incubation of 3 h with the different NPs suspension. After diffusion of DCFDA into the cell, this probe is deacetylated by intracellular ROS, forming 2', 7'-dichlorofluorescein (DCF). Since DCF is fluorescent, the fluorescence intensity of the samples is proportional to the ROS generation by NPs. This assay suggested that the ROS generation is not part of the main process of the mechanism of action of the NPs since ROS generation decreased from AuNPs to AuPtNPs and AgNPs which follows a trend contrary to the observed antimicrobial activity. The ROS generation by AgNPs was about 1.4 times lower in *P. aerug*inosa than AuNPs whereas the antimicrobial activity of AgNPs against this strain was about 10 times higher than AuNPs. Also, with the exception of the higher ROS generation by AuPtNPs in *S. aureus*, the results of ROS generation do not explain the enhanced antimicrobial activity of AuPtNPs in comparison with AuNPs.

Cell viability

Considering the unique performance of metallic NPs as antimicrobial agents and their increasing presence in our

Fig. 4 Fluorescence intensity measured after 3 h of incubation of each microorganism with the different types of NPs. Each type of NP was evaluated at the maximum concentration used in the antimicrobial assay: 0.96 mM, 0.20 mM, and 0.69 mM of AuNPs, AgNPs, and AuPtNPs, respectively. Cells incubated with the probe without the NPs were used as a negative control. λ_{Exc} 485 nm; λ_{Em} 528 nm

daily life, it is urgent to elicit their possible adverse effects on human health and environment. Although the toxicity of AgNPs has already been demonstrated in several animal models, AuNPs and AuPt NPs have been reported as biocompatible nanomaterials (Asharani et al. 2011; Arvizo et al. 2010; Zhao et al. 2014; Villiers et al. 2010). As already discussed above, the comparison between the published results about toxicity is hampered by several divergences among the physico-chemical characterization and units used to report colloidal concentration. Therefore, in this work, cell viability assays with Hs68 cells (Fig. 5) were performed in order to compare the cytotoxicity of AuNPs, AgNPs, and AuPtNPs at the concentration close to colloidal suspension resultant from the most commonly used synthetic routes. The cytotoxicity was evaluated at the concentration of the colloidal suspension (stock solution) and at two dilutions (Table 2). Considering that a material is cytotoxic only if the cell viability in its presence is lower than 60%, AuNPs and AuPt NPs were not toxic to Hs68 cells. As already expected, AgNPs was the most cytotoxic NPs, showing values of cell viability lower than 60% after all periods of incubation. The toxic effect was dose-dependent since the cell viability increased with the dilution of the NPs suspension. The AgNPs were not toxic only at the lower concentration that was tested, that was the stock suspension diluted 5× (0.07 mM) since the cell viability after all periods of incubation was about 80%.

In vivo assays with *Danio rerio*

Toxicity of AuNPs, AgNPs, and AuPtNPs was further investigated by in vivo assays with *Danio rerio* (zebrafish). The embryos were exposed to the NPs suspensions during 96 h and during this period the development of these embryos was evaluated regarding the hatching rate and coagulation of the eggs, malformation of larvae, mobility, and mortality. Figure 6 shows the overall analysis of the toxic effects observed for all the NPs. Representative pictures of embryos at different stage of development are shown in Figs. 7, 8, and 9 wherein it is also available detailed information about the effects observed after each period of incubation.
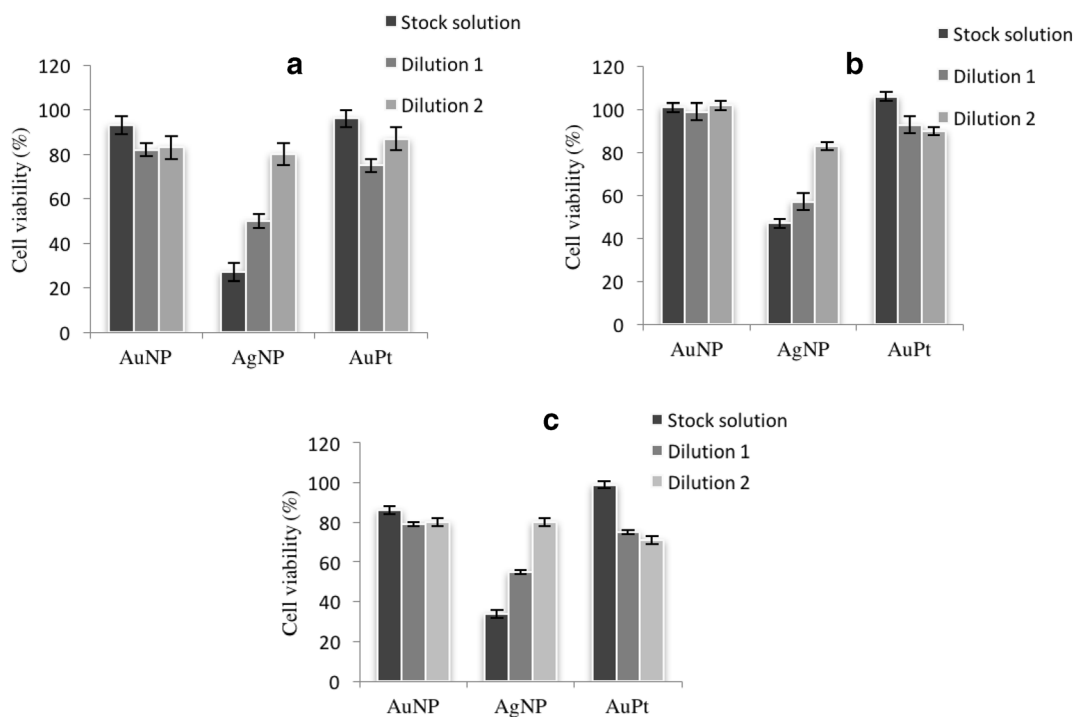
Fig. 5 Results of MTT cell viability assay after treatment of Hs68 cells with AuNPs, AgNPs, and AuPtNPs. *Error bars* represent the standard deviation. Significant difference was observed between different concentrations of AgNP and between AgNP data and the AuNP, AuPtNP data ($p < 0.05$). The different columns represent the different concentration according to Table 2. The cells were incubated with the samples for 24 h (**a**), 48 h (**b**), and 72 h (**c**)

In the presence of AuNPs at the higher concentration (stock solution), only 20% of the eggs coagulated after 48 h and 80% of the eggs generated normal larvae. When the AuNPs suspension was diluted, no toxic effects were observed during the total period of 96 h. The bimetallic AuPtNPs showed increased toxicity compared to AuNPs since embryo mortality was observed at all tested concentration. However, the toxicity was lower at the intermediary concentration (0.69 mM) which induced only 7% of mortality whereas the exposition to the lower concentration and stock solution resulted in 20% and 37% of embryos death, respectively. Surprisingly, the lower concentration (0.27 mM) showed higher toxicity by causing malformation of 33% of larvae. The higher toxicity of the less concentrated solution may be a result of the colloidal state of the NPs since in diluted suspension, the NPs are less prone to aggregated and as already discussed by other authors, the biological interaction, mainly with cell membrane, of NPs as individual particles differ from the interaction of NPs as aggregates. Once NPs are dispersed, they can penetrate cell membrane resulting in intracellular toxic effects. As already observed in the in vitro assays, AgNPs were the most toxic NPs. At all concentrations, AgNPs induced toxic effects after each period, from 24 h to 96 h of exposition. Coagulation of eggs and hatching delay were observed after 24 h and after 96 h the effects of the exposition to the stock solution were more severe. At this condition, 80% of the eggs were coagulated and the 20% of eggs generated larvae with slower motility.

These results are in line with the reported toxic effects on zebrafish published before. The low toxicity of AuNPs has already been reported regarding the insignificant number of observed dead embryos and larvae with malformation. Additionally, AuNPs were reported to induce embryos death only at 300 mg/mL. In contrast, the high toxicity of AgNPs was suggested by 100% of embryos death at 3 ug/mL. Toxicity assays with zebrafish had never been performed by using AuPtNPs but in a comparative study with AgNPs, AuNPs, and PtNPs, Asharani et al. (Asharani et al. 2011) reported an intermediary toxicity of PtNPs, which is in line with our results since AuPtNPs were more toxic than AuNPs but not as toxic as AgNPs.

Conclusions

The remarkable performance of metallic NPs as contrast and antimicrobial agents has motivated their application in industry and health fields. On the other hand, their wide application has increased the concerns regarding NPs toxicity to health and environment. Recent studies have reported bimetallic NPs as a biocompatible nanomaterial with satisfactory antimicrobial activity that could be used as antimicrobial agents as an alternative to metallic NPs. Nevertheless, the biocompatibility of bimetallic NPs has been suggested by a limited number of in vitro studies. Herein, the antimicrobial activity and toxicity of bimetallic NPs of gold and platinum have been evaluated in vitro and in vivo in comparative studies with AuNPs and AgNPs. In vivo studies with zebrafish have emerged as a valuable tool to assess nanotoxicity not only for being informative regarding the biochemical, physiological, and environmental aspects but also due to their genomic similarity to humans. However, toxicological studies performed until now used NPs suspension at colloidal states different from the stock suspension obtained from the synthetic route. Although this is a methodology commonly used in pharmacology when the focus is comparing doses, from

Fig. 6 Percentage of dead, normal, and abnormal embryos of zebrafish observed after 96 h of exposition to NPs at different concentrations. Each type of NP was evaluated at the concentration of stock suspension and at two different dilutions. The concentrations are depicted in Table 2
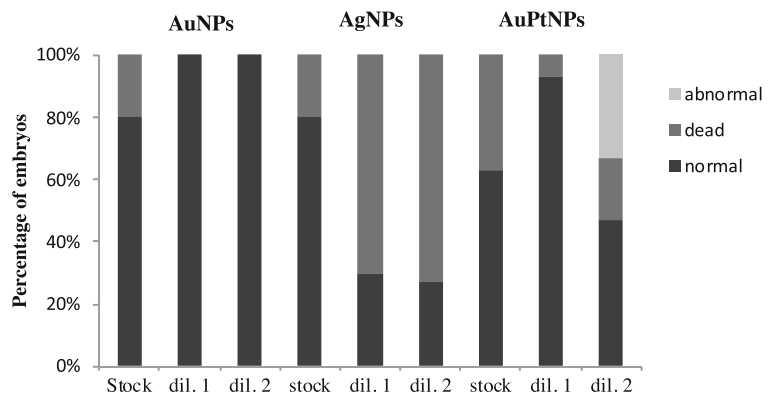
the physicochemical point of view, when comparing NPs suspension, concentration/dilution procedure starting from a stock suspension, induces the destabilization of NPs suspension. Therefore, despite the differences regarding the size and concentration of the NPs used in this work, the comparison between them is valuable in order to assess the advantages and the risks of their application at the colloidal state resultant from the usual synthetic routes.

The antimicrobial activity of AgNPs was superior to the activity of AuNPs and AuPtNPs. Notoriously, the activity of AuPtNPs very similar to the activity of AgNPs regarding the inhibition growth of *S. aureus*. However, AgNPs were shown to be very cytotoxic to HS68 cells. The toxicity of AgNPs was also observed in vivo, resulting in high mortality and malformation of zebrafish larvae. On the other hand, AuNPs were not cytotoxic and presented the lowest toxicity against zebrafish. The death
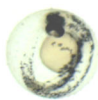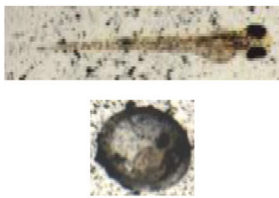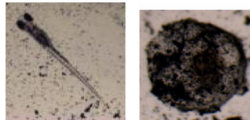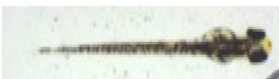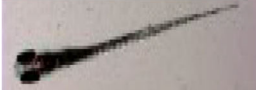
AuNPs			
24h	48h	72h	96h
Control N = 15; 100% Normal development	N = 15; 87% Normal 13% larvae without hatching, but normal	N = 15; 100% Normal development	N = 15; 100% Normal development
stock N = 17; 100% Normal development	N = 17; 59% Normal 41% larvae without hatching, but normal	N = 17; 80% Normal development 20% clotted	N = 17; 80% Normal development 20% clotted
dilution 1 N = 17; 100% Normal development	N = 17; 87% Normal 13% larvae without hatching, but normal	N = 17; 100% Normal development	N = 17; 100% Normal development
dilution 2 N = 15; 100% Normal development	N = 15; 87% Normal and 13% larvae without hatching, but normal	N = 15; 100% Normal development	N = 15; 100% Normal development

Fig. 7 Representative pictures of zebrafish eggs and embryos exposed to AuNPs at different concentrations (Table 2) during 96 h
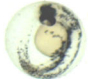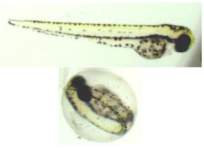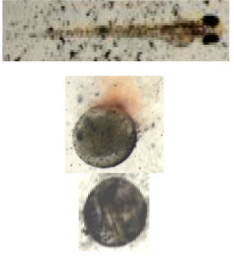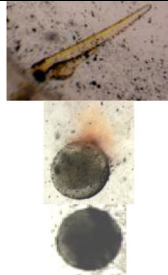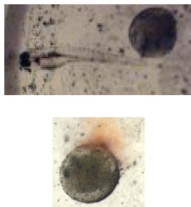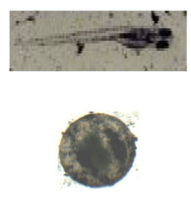
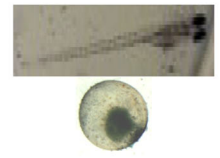|	AgNPs			
	24h	**48h**	**72h**	**96h**
Control	100% Normal development	87% Normal 13% eggs not hatched, but normal aspect	100% Normal development	100% Normal development
stock	50% clotted 20% delay in the development 30% normal development	80% clotted 7% eggs not hatched, but normal aspect 13% normal development	80% clotted 20% normal development	80% clotted 20% normal larvae but slow locomotion
dilution 1	47% clotted 20% delay in the development 33% normal development	70% clotted 18% eggs not hatched 12% normal development	70% clotted 30% normal development	70% clotted 30% normal larvae but slow locomotion
dilution 2	14% clotted 86% normal development	27% clotted 67% eggs not hatched but with normal aspect 6% normal development	27% clotted 73% normal development	27% clotted 73% normal development

Fig. 8 Representative pictures of zebrafish eggs and embryos exposed to AgNPs at different concentrations (Table 2) during 96 h. In each assay, $N = 15$

rate was of only 20% after 24 h at the highest AuNPs concentration which corresponds to the stock suspension. Although the presence of Pt in the NP had enhanced antimicrobial activity in comparison to AuNPs, this advantage was accompanied by the counterpoint of higher cytotoxicity and toxic effects. Although bimetallic NPs have been reported as materials of enhanced biocompatibility in comparison with metallic NPs, herein AuPtNPs showed significant toxicity. The exposition of zebrafish embryos to stock suspension induced death of 37% of the embryos and 33% of malformation of larvae. A comprehensive study regarding the toxicity of these NPs requires further assays, especially to elicits the mechanism of action in microbial and mammalian cells.
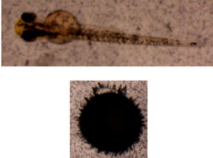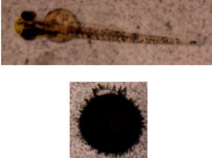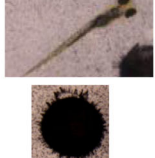
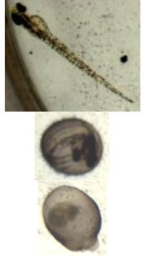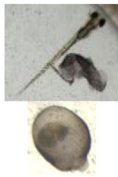| AuPtNPs | | | |
24h	48h	72h	96h
Control N = 15; 100% Normal development	N = 15; 87% Normal 13% larvae without hatching, but normal	N = 15; 100% Normal development	N = 15; 100% Normal development
Stock N = 15; Apparently all normal	N = 15; 37% clotted 63% Normal larvae development	N = 15; 37% clotted 63% Normal larvae development	N = 15; 37% clotted 63% Normal larvae development
dilution 1 N = 15; Apparently all normal	N = 15; 93% eggs without hatching, but normal 7% Normal larvae development	N = 15; 93% eggs without hatching, but normal 7% Normal larvae development	N = 17; 93% eggs without hatching, but normal 7% Normal larvae development
dilution 2 N = 15; Apparently all normal	N = 15; 20% clotted 73% eggs without hatching, but normal 7% Normal larvae development	N = 15; 20% clotted 33% abnormal larvae development (column) 47% Normal larvae development	N = 15; 20% clotted 33% abnormal larvae development (column) 47% Normal larvae development

Fig. 9 Representative pictures of zebrafish eggs and embryos exposed to AuPtNPs at different concentrations (Table 2) during 96 h

Compliance with ethical standards

Conflict of interest   The authors declare that there is no conflict of interest.

References

Aioub M, Panikkanvalappil SR, El-Sayed MA (2017) Platinum-coated gold nanorods: efficient reactive oxygen scavengers that prevent oxidative damage toward healthy, untreated cells during plasmonic photothermal therapy. ACS Nano 11:579–586

Arvizo R, Bhattacharya R, Mukherjee P (2010) Gold nanoparticles: opportunities and challenges in nanomedicine. Expert Opin Drug Deliv 7:753–763

Asharani P, Lianwu Y, Gong Z, Valiyaveettil S (2011) Comparison of the toxicity of silver, gold and platinum nanoparticles in developing zebrafish embryos. Nanotoxicology 5:43–54

Ávalos Fúnez A, Isabel Haza A, Mateo D, Morales P (2013) In vitro evaluation of silver nanoparticles on human tumoral and normal cells. Toxicol Mech Methods 23:153–160

Busquet F, Strecker R, Rawlings JM, Belanger SE, Braunbeck T, Carr GJ, Cenijn P, Fochtman P, Gourmelon A, Hübler N, Kleensang A, Knöbel M, Kussatz C, Legler J, Lillicrap A, Martínez-Jerónimo F, Polleichtner C, Rzodeczko H, Salinas E, Schneider KE, Scholz S, van den Brandhof EJ, van der Ven LTM, Walter-Rohde S, Weigt S, Witters H, Halder M (2014) OECD validation study to assess intra-and inter-laboratory reproducibility of the zebrafish embryo toxicity test for acute aquatic toxicity testing. Regul Toxicol Pharmacol 69:496–511

Conceição K, Monteiro-dos Santos J, Seibert CS, Silva PI Jr, Marques EE, Richardson M, Lopes-Ferreira M (2012) Potamotrygon cf. henlei stingray mucus: biochemical features of a novel antimicrobial protein. Toxicon 60:821–829

Dakal T.C.; Kumar A.; Majumdar R.S.; Yadav V. 2016 Mechanistic basis of antimicrobial actions of silver nanoparticles. Front Microbiol, 7.

Enustun B, Turkevich J (1963) Coagulation of colloidal gold. J Am Chem Soc 85:3317–3328

Feng ZV, Gunsolus IL, Qiu TA, Hurley KR, Nyberg LH, Frew H, Johnson KP, Vartanian AM, Jacob LM, Lohse SE et al (2015) Impacts of gold nanoparticle charge and ligand type on surface binding and toxicity to Gram-negative and Gram-positive bacteria. Chem Sci 6:5186–5196

Gao X, Topping VD, Keltner Z, Sprando RL, Yourick JJ (2017) Toxicity of nano- and ionic silver to embryonic stem cells: a comparative toxicogenomic study. J Nanobiotechnol 15:31

Gorup LF, Longo E, Leite ER, Camargo ER (2011) Moderating effect of ammonia on particle growth and stability of quasi-monodisperse silver nanoparticles synthesized by the Turkevich method. J Colloid Interface Sci 360:355–358

Haiss W, Thanh NT, Aveyard J, Fernig DG (2007) Determination of size and concentration of gold nanoparticles from UV- Vis spectra. Anal Chem 79:4215–4221

Hinterwirth H, Lindner W, Lämmerhofer M (2012) Bioconjugation of trypsin onto gold nanoparticles: effect of surface chemistry on bioactivity. Anal Chim Acta 733:90–97

Howe K, Clark MD, Torroja CF, Torrance J, Berthelot C, Muffato M, Collins JE, Humphray S, McLaren K, Matthews L et al (2013) The zebrafish reference genome sequence and its relationship to the human genome. Nature 496:498

Jung WK, Koo HC, Kim KW, Shin S, Kim SH, Park YH (2008) Antibacterial activity and mechanism of action of the silver ion in Staphylococcus aureus and Escherichia coli. Appl Environ Microbiol 74:2171–2178

Kaiser JP, Roesslein M, Diener L, Wichser A, Nowack B, Wick P (2017) Cytotoxic effects of nanosilver are highly dependent on the chloride concentration and the presence of organic compounds in the cell culture media. J Nanobiotechnology 15:5

Kim JS, Sung JH, Ji JH, Song KS, Lee JH, Kang CS, Yu IJ (2011) In vivo genotoxicity of silver nanoparticles after 90-day silver nanoparticle inhalation exposure. Saf Health Work 2:34–38

Kumar S.; Mukherjee M.M.; Varela M.F. 2013 Modulation of bacterial multidrug resistance efflux pumps of the major facilitator superfamily. Int J Bacteriol.

Lai F, Chou H, Sarma LS, Wang D, Lin Y, Lee J, Hwang BJ, Chen C (2010) Tunable properties of Pt_xFe_{1-x} electrocatalysts and their catalytic activity towards the oxygen reduction reaction. Nanoscale 2:573–581

Lapp AS, Duan Z, Marcella N, Luo L, Genc A, Ringnalda J, Frenkel AI, Henkelman G, Crooks RM (2018) Experimental and Theoretical Structural Investigation of AuPt Nanoparticles Synthesized Using a Direct Electrochemical Method. J Am Chem Soc 140, 20:6249–6259

Linic S, Aslam U, Boerigter C, Morabito M (2015) Photochemical transformations on plasmonic metal nanoparticles. Nat Mater 14:567–576

Ma Y, Song L, Lei Y, Jia P, Lu C, Wu J, Xi C, Strauss PR, Pei DS (2018) Sex dependent effects of silver nanoparticles on the zebrafish gut microbiota. Environ Sci: Nano 5:740–751

McShan D, Ray PC, Yu H (2014) Molecular toxicity mechanism of nanosilver. J Food Drug Anal 22:116–127

Mott D, Luo J, Smith A, Njoki PN, Wang L, Zhong C (2007) Nanocrystal and Surface alloy properties of bimetallic Gold-Platinum nanoparticles. Nanoscale Res Lett 2:12–16

Murphy S, Murphy CJ, Leach A, Gall KA (2015) Possible oriented attachment growth mechanism for silver nanowire formation. Cryst Growth Des 15(4):1968–1974

Paramelle D, Sadovoy A, Gorelik S, Free P, Hobley J, Fernig DG (2014) A rapid method to estimate the concentration of citrate capped silver nanoparticles from UV-visible light spectra. Analyst 139:4855–4861

Park SB, Steadman CS, Chaudhari AA, Pillai SR, Singh SR, Ryan PL, Willard ST, Feugang JM (2018) Proteomic analysis of antimicrobial effects of pegylated silver coated carbon nanotubes in Salmonella enterica serovar Typhimurium. J Nanobiotechnol 16:31

Penn RL, Banfield JF (1998) Imperfect oriented attachment: dislocation generation in defect-free nanocrystals. Science 281: 969–971

Petkov V, Wanjala BN, Loukrakpam R, Luo J, Yang L, Zhong C, Shastri S (2012) Pt-Au Alloying at the nanoscale. Nano Lett 12(8):4289–4299

Qian H, Zhao Q, Dai B, Guo L, Zhang J, Liu J, Zhang J (2015) Oriented attachment of nanoparticles to form micrometer-sized nanosheets/nanobelts by topotactic reaction on rigid/flexible substrates with improved electronic properties. NPG Asia Mater 7:e152

Qingbo Z, Jianping X, Yue Y, Jim Y (2010) L. Monodispersity control in the synthesis of monometallic and bimetallic quasi-spherical gold and silver nanoparticles. Nanoscale 2:1962–1975

Raju M, van Duin ACT, Fichthorn KA (2014) Mechanisms of oriented attachment of TiO2 nanocrystals in vacuum and humid environments: reactive molecular dynamics. Nano Lett. 14:1836–1842

Siddiqi KS, Husen A, Rao RAK (2018) A review on biosynthesis of silver nanoparticles and their biocidal properties. J Nanobiotechnol 16:14

Sieber S, Grossen P, Detampel P, Siegfried S, Witzigmann D, Huwyler J (2017) Zebrafish as an early stage screening tool to study the systemic circulation of nanoparticulate drug delivery systems in vivo. J Control Release 264:180–191

Singh J, Dutta T, Kim K, Rawat M, Samddar P, Kumar P (2018) "Green" synthesis of metals and their oxidenanoparticles: applications for environmental remediation. J. Nanobiotechnol. 16:84

Smith L, Kuncic Z, Ostrikov K, Kumar S (2012) Nanoparticles in cancer imaging and therapy. J Nanomater 2012:10

Song K, Xu P, Meng Y, Geng F, Li J, Li Z, Xing J, Chen J, Kong B (2013) Smart gold nanoparticles enhance killing effect on cancer cells. Int J Oncol 42:597–608

Srinoi P, Chen YT, Vittur V, Marquez MD, Lee TR (2018) Bimetallic nanoparticles: enhanced magnetic and optical properties for emerging biological applications. Appl Sci 8: 1106

Tian X, Jiang X, Welch C, Croley TR, Wong TY, Chen C, Fan S, Chong Y, Li R, Ge C et al (2018) Bactericidal effects of silver nanoparticles on lactobacilli and the underlying mechanism. ACS Appl Mater Interfaces 10:8443–8450

Uson L, Sebastian V, Mayoral A, Hueso JL, Eguizabal A, Arruebo M, Santamaria J (2015) Spontaneous formation of Au–Pt alloyed nanoparticles using pure nano-counterparts as starters: a ligand and size dependent process. Nanoscale 7: 10152–10161

Van Pomeren M, Brun N, Peijnenburg W, Vijver M (2017) Exploring uptake and biodistribution of polystyrene (nano) particles in zebrafish embryos at different developmental stages. Aquat Toxicol 190:40–45

Villiers CL, Freitas H, Couderc R, Villiers MB, Marche PN (2010) Analysis of the toxicity of gold nanoparticles on the immune system: effect on dendritic cell functions. J Nanopart Res 12: 55–60

Wang L, Hu C, Shao L (2017) The antimicrobial activity of nanoparticles: present situation and prospects for the future. Int J Nanomed 12:1227

Westsson E, Koper GJ (2014) How to determine the core-shell nature in bimetallic catalyst particles? Catalysts 4:375–396

Xu Y, Chen L, Wang C, Yao W, Zhang Q (2015) Recent advances in noble metal based composite nanocatalysts: colloidal synthesis, properties, and catalytic applications. Nanoscale 7: 10559–10583

Yao C, Zhang L, Wang J, He Y, Xin J, Wang S, Xu H, Zhang Z (2016) Gold nanoparticle mediated phototherapy for cancer. J Nanomater 2016

Zhao L, Heinig N, Leung KT (2013) Formation of Au−Pt Alloy nanoparticles on a Si substrate by simple dip-coating at room temperature. Langmuir 29:927–931

Zhao Y, Ye C, Liu W, Chen R, Jiang X (2014) Tuning the composition of AuPt bimetallic nanoparticles for antibacterial application. Angew Chem Int Ed 53:8127–8131

Zhong C, Luo J, Njoki PN, Mott D, Wanjala B, Loukrakpam R, Lim S, Wang L, Fang N, Xu Z (2008) Fuel cell technology: nano-engineered multimetallic catalysts. Energy Environ Sci 1:454–466

Zhou Y, Kong Y, Kundu S, Cirillo JD, Liang H (2012) Antibacterial activities of gold and silver nanoparticles against Escherichia coli and bacillus Calmette-Guérin. J Nanobiotechnology 10:1